Fusion Engineering and Design 201 (2024) 114228

Contents lists available at ScienceDirect

Fusion Engineering and Design

journal homepage: www.elsevier.com/locate/fusengdes

Thermal and structural analyses on different mirrors of the Multi-Beam Transmission Line of DTT ECH system

A. Salvitti [a,*], A. Bruschi [b], G. Calabrò [a], F. Fanale [c,d], P. Fanelli [a], S. Garavaglia [b], G. Granucci [b], S. Meloni [a], A. Moro [b], P. Platania [b], A. Romano [c,d], M. Scungio [a]

[a] Department of Economy, Engineering, Society and Business Organization (DEIM), University of Tuscia, Largo dell'Università, Viterbo 01100, Italy
[b] Institute for Plasma Science and Technology, National Research Council (ISTP-CNR), Via Cozzi 53, 20125 Milan, Italy
[c] DTT S.C.a r.l., Via E. Fermi 45, I-00044, Frascati Roma, Italy
[d] ENEA, Fusion and Nuclear Safety Department, C.R. Frascati, Via E. Fermi 45, 00044 Frascati, Roma, Italy

ARTICLE INFO

Keywords:
ECH
MBTL
Mirror
Thermal-Structural analysis
Temperature
Deformation

ABSTRACT

To achieve efficient power transfer, the Divertor Tokamak Test (DTT) facility relies on supplementary heating systems. One of them is the Electron Cyclotron Heating (ECH). ECH employs 4 clusters, each comprising 8 gyrotrons as Radio Frequency (RF) sources, 1 quasi-optical Multi-Beam Transmission Line (MBTL), and 8 independent launchers. The generated RF power (170 GHz, 1 MW, 100 s) is delivered to the plasma through oversized flat and focusing mirrors. However, the MBTL faces challenges during operation as the microwave beams reflected from the mirror contribute to its heating, absorbing a fraction of the beam power (0.06–0.2 MW/m^2). Consequently, mirrors temperature rises, causing thermal expansion-induced deformations that reduce the transmission line efficiency. To address this issue, the mirrors must be designed with careful consideration of their thermal and structural properties to maintain optimal optical performance. This work presents the conceptual design of various actively cooled flat and parabolic MBTL mirrors, using thermo-structural finite element simulations. The performed analyses aim to examine the distinct thermo-structural characteristics of different mirrors and reconstruct the deformed reflective surfaces. The studied mirrors are divided into two types, based on the position in the TL. The mirror temperatures and total deformations resulting from the simulations do not exceed 41 °C and 0.13 mm, respectively. The deformed reflective profiles can then be used to assess the TL losses, exporting the surfaces, and implementing them in the overall electromagnetic model of the line.

1. Introduction

The Divertor Tokamak Test (DTT) facility is an Italian project, designed to explore alternative power-exhaust solutions [1]. The Electron Cyclotron Heating (ECH) [2–3] is one of the DTT external heating systems expected to provide part of 45 MW of additional power needed for the plasma. The ECH system comprises 4 clusters, each consisting of 8 gyrotrons (Radio-Frequency sources), a quasi-optical Transmission Line (TL) and 8 independent antennae [4–7].

The central section of this system is the TL. Its function is to guide the microwave beams generated by the gyrotrons towards the plasma. It can be conceptually divided into three main segments: Single-Beam (SB) TL gyrotron-side, Multi-Beam TL (MBTL) along an elevated corridor connecting the gyrotron hall to the tokamak hall, SBTL torus-side.

In this framework the present paper focuses on the MBTL, the majority of which is housed inside a corridor in a dedicated building, while the initial and final sections extend into the gyrotron building and the torus hall, respectively.

The TL has two main characteristics: it is designed to be completely quasi-optical, drawing inspiration from the successful experience of W7-X [8–9], and evacuated, to reduce losses and risk of arcing in air [3–7]. The power transmission from the gyrotron to the launcher is fully based on the propagation of Gaussian beams, following quasi-optical propagation laws [10]. The MBTL, on average 100 m long depending on the cluster considered [3], is composed of flat and focusing Multi-Beam Mirrors (MBMs). In Fig. 1 an example of a unit of mirrors of the MBTL is represented, with the four-mirrors arranged in a dogleg configuration and 90° reflections [8]. The flat MBMs act only in modifying the propagation direction of the beams. The surface of focusing MBMs is parabolic, necessary to refocusing the beams. Given that the parabolic

* Corresponding author.
E-mail address: alessandra.salvitti@unitus.it (A. Salvitti).

https://doi.org/10.1016/j.fusengdes.2024.114228
Received 13 October 2023; Received in revised form 16 January 2024; Accepted 5 February 2024
Available online 23 February 2024

mirrors have to be placed at a fixed distance equal to twice the focal length, a path including only parabolic mirrors without flat mirrors would require unfeasible space occupation.

Throughout the entire MBTL path, eight distinct microwave beams are simultaneously reflected by a single metallic mirror. The mm-wave beam of 1 MW of power is produced by the gyrotron. Despite the mirror's high reflection efficiency, a small portion (approximately 0.14–0.16 %) of the incident beam power is absorbed by the mirror's surface due to Ohmic losses.

During operation, which involves a 100 s pulse every hour, the mirror's temperature rises, leading to deformations that result in reduced transmission efficiency. The TL has the objective to transmit the beams with the minimum losses or distortion, in order to couple at least 85 % of the power into the plasma. One of the main contributions to the losses is the degradation of quality of the beam during the propagation up to the end of the line. The deformations of the mirrors are one of the causes of this kind of losses.

To address this issue, the conceptual design of various water-cooled MBMs, both flat and parabolic, is undertaken, and their thermal-structural behaviour is simulated. The current work extends the preliminary study of the parabolic mirror design presented in [11], completing the line with the analysis of all its mirrors.

The presented analysis focuses on examining the distinct thermo-structural characteristics across different types of mirrors, analysing which of them exhibits worse conditions. The results reported here allow to reconstruct the deformed reflective surfaces, which is crucial for evaluating the impact of these deformations on the performance of the TL [6].

2. MBTL mirrors

2.1. Models

In this paper two different types of MBMs are considered:

- type 1 (TY1): the mirrors located at the midsection of the MBTL. This typology is found in the midsection of the TL, like the one shown in Fig. 1
- type 2 (TY2): the mirrors positioned at the beginning and the end of the MBTL. This typology can be found in the sections of the TL connecting the MBTL to the SBTLs in the gyrotron hall and in the DTT hall.

Both types of mirrors encompass a combination of focusing and flat mirrors. The flat mirrors differ in the thermal loading distribution depending on the propagation path of the beams between two focusing mirrors: parallel (P) or crossing (C), as visible in Fig. 1. The sequence of crossing and parallel beams is inherent in the confocal arrangement, the only one which helps in reducing the transmission losses. It is mandatory to have parallel beams at the input and output of a transition from SB to MB lines, where it is necessary to have the beam spots smaller and separated. In the crossing part, the beams are always superimposed. The transition from TY1 to TY2 (and vice versa), with different focal length, is conveniently realised where the beams are crossing.

The basic shape of the mirrors is elliptical. The dimensions are reported in the Table 1.

As already mentioned, the conceptual design of these mirrors starts from the outcomes presented in [11].

Each MBM consists of two distinct components: a bulk and an upper layer, both in pure Copper (Cu), with constant thickness for the flat mirrors or with parabolic curvature, in the case of focusing mirrors. The process for achieving the parabolic curvature is described in [11], considering different focal lengths. The thickness of the bulk is 1.6 cm, and the minimum thickness of the upper layer is 4 mm (Fig. 2).

The bulk is dug with the cooling channels, in which the water flows to refrigerate the structures. This cooling approach, as reported in [11] and already studied in W7-X [12–14], features elongated spiral-shaped channels. This design enables high efficiency of cooling, well covering the entire reflective surface.

For the sake of clarity, in Fig. 3 a specific example of the cooling channels, integrated into the bulk of a parabolic mirror, is represented. The inlet is strategically located near the peak of the thermal load, which is not in the mirror centre, being characterized by the 8 beams distribution over the mirror surface. Here the flow rate is divided into two distinct paths, one directed towards the centre of the mirror and the other outwards. Consequently, the mirror has two parallel cooling channels, each featuring a semicircular cross-section.

The mass flow rate is divided such that the pressure drops are equal in the internal and the external channels, using the same method presented in [11]. From this condition, the diameters of the channels are determined. Specifically, the internal diameter is equal for TY1 and TY2 MBMs and it is 12 mm. On the other hand, the external diameters are 15 mm for TY1 and 16 mm for TY2. The difference arises from the different channel lengths, due to different geometries of the mirrors (with TY2 mirrors smaller than TY1).

The unequal geometries and different thermal loads, which will be discussed in the next paragraph, lead to different spiral definitions. Specifically, spirals are designed by a parametric equation function of the angle of the polar coordinate system. The pitch of the spiral is 3 cm

Table 1
Geometrical data of the mirrors of TY1 and TY2.

Geometrical data (TY1)	Focal Length	Minor radius	Major radius
PARABOLIC	2850 mm	380 mm	537 mm
FLATs	/	350 mm	495 mm
Geometrical data (TY2)	**Focal Length**	**Minor radius**	**Major radius**
PARABOLIC	2300 mm	350 mm	495 mm
FLATs	/	325 mm	460 mm

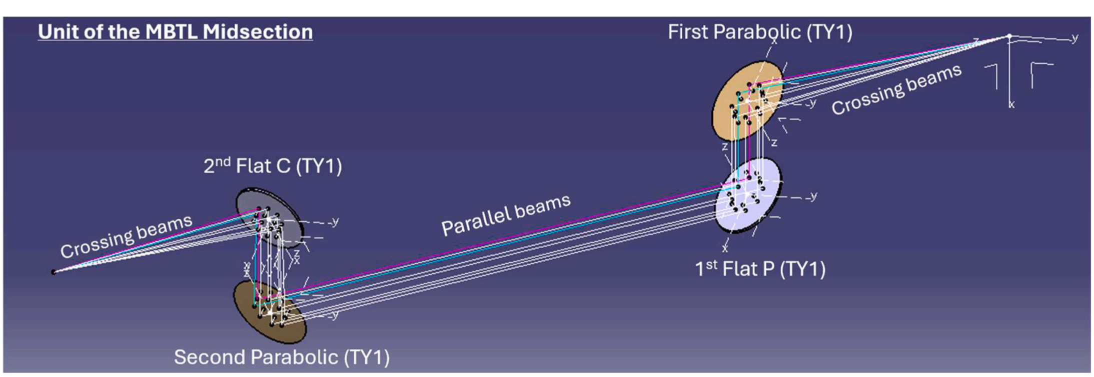

Fig. 1. Example of a unit of the midsection of the MBTL, with 4 reflecting mirrors (2 focusing and 2 flat mirrors). Two units form the whole midsection.

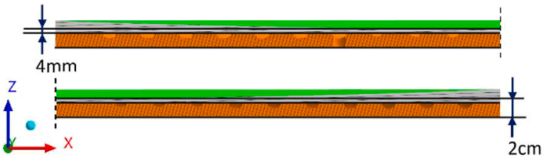

Fig. 2. Section view of a parabolic mirror. In orange the bulk, in grey the upper layer, in green the reflective parabolic surface.

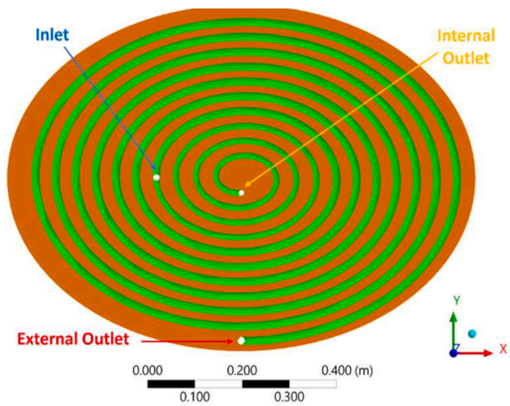

Fig. 3. Example of the cooling channels in the bulk of a parabolic mirror.

on the x-axis and 3 cm multiplied by the ratio of the radii of the mirror on the y-axis. The angular ranges change in accordance with the mirror dimensions for each configuration.

2.2. Thermal load

The mirrors inside a vacuum envelope are mainly subject to the microwave load, which comes from the absorption fraction of the incident power transported by the beams, whose power density in the transverse section has a circularly symmetric gaussian shape.

The thermal load related to the microwave beam is a surface load, defined considering a Gaussian distribution of power in the beams, with size defined according to the TL design. The formulations are the same used in [11], but some conditions have been updated: the new total power of a single gyrotron beam is $Q = 1$ MW; the projected beams widths ($w_x^{'}$ and $w_y^{'}$ along the x and y mirror directions) and the new absorption coefficients (A) are reported in Table 2. The absorption coefficient has changed, now considering more realistic polarization of the propagating beam, instead of the worst case (with $A = 0.21$ %) found in [11]. As the beam polarization changes along the propagation, "A" varies depending on different mirrors. In the table, the last column reports the peak value of the total absorbed heat flux, already considering the bundle of beams.

The total absorbed microwave power to be removed is in the range 11.2–12.8 kW.

The microwave load differs for each mirror not only in the parameters reported in Table 2, but also in the location of the centre of the beams on the reflective surface. For brevity only two indicative plots are reported in Fig. 4: the 1st flat P mirror TY1 and the 3rd flat C mirror TY2. They represent two opposite configurations, with beams more distant (Fig. 4, left) and closer to each other (Fig. 4, right).

Table 2
Microwave load parameters.

	$w_x^{'}$ $[m]$	$w_y^{'}$ $[m]$	A	$P_{abs\ MAX}$ $[W/m^2]$
PARAB. (TY1)	0.15040	0.10635	0.14 %	63755
1st FLAT P (TY1)	0.12654	0.08948	0.14 %	82372
2nd FLAT C (TY1)	0.14827	0.10484	0.14 %	76373
PARAB. (TY2)	0.14808	0.10471	0.15 %	83599
1st FLAT P (TY2)	0.08344	0.05900	0.16 %	207950
2nd FLAT P (TY2)	0.11062	0.07822	0.16 %	126426
3rd FLAT C (TY2)	0.14602	0.10325	0.16 %	117604

3. Finite Element models

The mirrors are studied with Finite Element (FE) analyses, using the Software ANSYS. Transient thermal and structural simulations are carried out, studying the evolution of the mirror temperature and deformations for 150 s, including the 100 s pulse duration. The initial 10 s are used to stabilize the simulation. Successively, after 10 s, the thermal load is activated for 100 s, at 110 s the load is deactivated, and the water continues to cool the structure.

The FE approach is aligned with the methodology used in [11] and [15]. The fluid thermal element FLUID116 has been employed to simulate the fluid behaviour. This element allows for representing the mass and heat transport, and convection effects, with a simplified methodology, thus without resorting to computational fluid-dynamic analyses. The convection heat transfer coefficient (HTC) is calculated using the "Dittus-Boelter" formulation and it is assumed constant in both time and space, on the basis of low temperature gradients and conservative approximation.

Mesh models are predominantly structured with a high degree of refinement, as depicted in Fig. 5. They have undergone a mesh sensitivity analysis, leading to an average of $2.5 \cdot 10^5$ elements and $3.0 \cdot 10^5$ nodes. Linear elements, primarily hexahedrons, were predominantly used in this mesh refinement process.

The input parameters of the thermal analysis are:

- water inlet temperature $T_{water\ (inlet)} = 15^{\circ}C$ (different from the previous condition reported in [11], according to the DTT water cooling system)
- water inlet pressure: $p_{water\ (inlet)} = 10\ bar$ (conservative value considering possible high pressure drops in the whole circuit)
- volumetric flow rate: see Table 3
- heat transfer coefficient: see Table 3

The volumetric flow rate and the HTC vary based on the type of mirror, due to different geometrical channel-sections.

The boundary conditions of the structural analysis are:

- the temperature distribution at each time-step of analysis;
- the water pressure on the channel walls (maintained conservatively constant at 10 bar);
- the forces at the inlet and the outlet that simulate the continuity of the flow.

The constraint is an equivalent support simulating a spherical joint

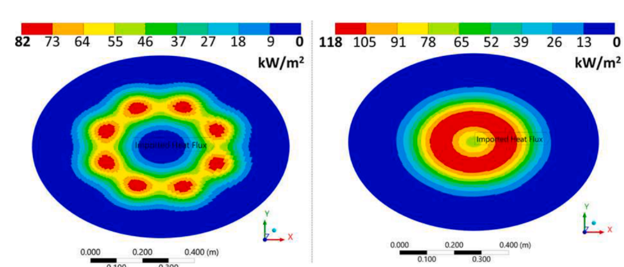

Fig. 4. Contour plot of the heat flux of the microwave load for the 1st flat P mirror TY1 (left) and for the 3rd flat C mirror TY2 (right).

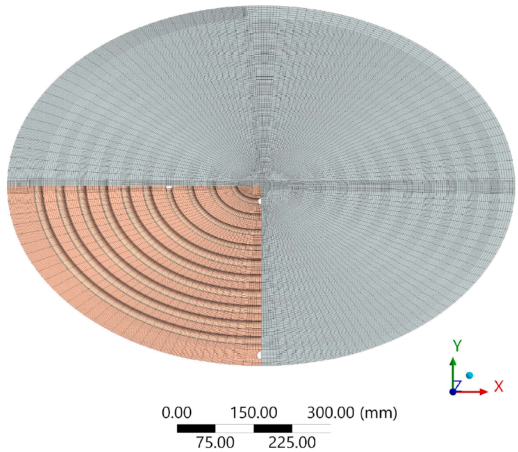

Fig. 5. Mesh model of the parabolic mirror TY2: in the bottom left corner, the detail of the mesh of the bulk with the channel.

Table 3
Volumetric flow rates and HTC values.

	$\dot{V}[l/\min]$		HTC $[W/(m^2K)]$	
	Internal Spiral	**External Spiral**	**Internal Spiral**	**External Spiral**
TY 1	10.2	10.3	11000	7500
TY 2	10.9	9.0	12000	6200

on the centre of the back of the mirror, as detailed in [11].

4. Results

Results are split into two different comparisons:

1) Comparing the mirrors of the same type (TY1 or TY2).
2) Comparing the same configurations of different types (Parabolic, Flat P and Flat C).

For the sake of brevity, it is chosen to analyse the thermal and structural results together, whereas directly connected.

4.1. Thermal and structural results

The first part of the reported results refers to the instant at the end of the pulse, so after 100 s from the activation of the load. This is a particular snapshot that plays a key role in the analysis. From a thermal perspective, it identifies the maximum temperature values on the mirrors, from a structural viewpoint, it finds the relative maxima of the maximum total deformation on the mirror. The total deformation is calculated as the root of the sum of squares of the x-y-z directional components. As will be illustrated in Fig. 7, the end of the pulse is not always the point with the highest total deformation. However, it is unequivocally the point at which the deformation reaches maximum values under stable conditions. It is worth noting that initial peaks related to the transitory are not considered, indeed they are influenced by a rapid variation of the thermal load, not relevant in the current study.

Referring to Table 4, as well as Figs. 6 and 7, it is possible to analyse some results. Table 4 provides the maximum temperature and total deformation values of the mirrors, while Figs. 6 and 7 illustrate the trends of the maximum temperature and total deformation over time for all the configurations. For the sake of clarity, trends related to TY2 are represented with solid lines while TY1 trends are indicated with dashed lines.

First of all, it is important to note the improvement of the parabolic

Table 4
Maximum temperatures and total deformations for all the mirrors at the end of the pulse.

End of the pulse	Max Temperature	Max Total Deformation
PARAB. (TY1)	26.9 °C	0.065 mm
1st FLAT P (TY1)	28.7 °C	0.100 mm
2nd FLAT C (TY1)	32.3 °C	0.091 mm
PARAB. (TY2)	30.7 °C	0.087 mm
1st FLAT P (TY2)	41.1 °C	0.126 mm
2nd FLAT P (TY2)	35.8 °C	0.125 mm
3rd FLAT C (TY2)	41.3 °C	0.114 mm

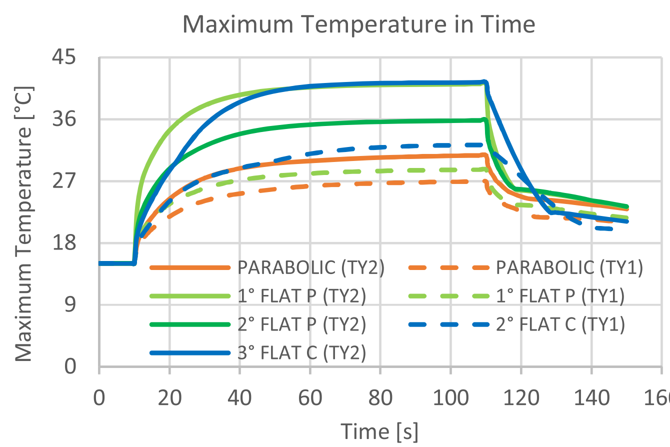

Fig. 6. Comparison of the trends of the maximum temperature over time for TY1 and TY2 mirrors.

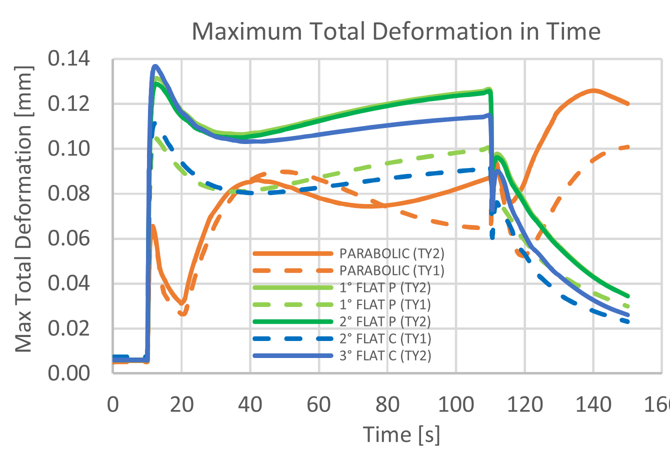

Fig. 7. Comparison of the trends of the maximum total deformation over time for TY1 and TY2 mirrors.

mirror TY1 compared to the last analysis in [11]: due to the change of Q, A and $T_{water\ (inlet)}$, the maximum mirror temperature and the maximum total deformation (end of the pulse) decrease by 28 °C and 0.075 mm, respectively.

It is noteworthy that the maximum temperatures of the mirrors do not exceed ~41 °C. The temperature results show all mirrors reach the maximum temperature almost steadily at the end of the pulse, instead, the temperature distribution is still changing. It is worth noting that trends of the total deformation are similar for flat mirrors and different for the parabolic ones, due to the greater distribution of the mass on the edge, caused by the parabolic shape. Moreover, the maximum total deformation does not overcome 0.13 mm.

In the first comparison 1), it is evident that in TY1 the 2nd flat mirror C exhibits the highest maximum temperature (32.3 °C), despite the maximum heat flux peak (Table 2) is relative to the parallel configuration. This result is due to the tighter bundle of the beams in the crossing configuration. With regard to the structural results, the highest value of the maximum total deformation is recorded in the 1st flat P mirror. This is ascribed to the greater influence on the deformation of the global temperature gradient, along thickness and radius, with respect to local ones.

The parabolic mirror, characterized by a lower heat flux, a higher stiffness on the edge (given by the curvature) and larger dimensions, exhibits a 35 % reduction in the maximum total deformation.

In TY2 it is noteworthy that the mirror with the highest maximum temperature remains the crossing one, with a similar value to the 1st mirror P. Indeed, the highest heat flux is relative to the parallel one, but, also here, the concentration of the beams in the crossing configuration leads to high temperature. Nevertheless, it is important to highlight that the highest maximum total deformation is found for the parallel configuration.

When examining the trends of the two flat P mirrors (Fig. 7) their behaviour is very similar, despite the differences in their maximum temperature trends. Instead, as for TY1, the parabolic mirror presents the lowest total deformation values.

In the second comparison 2), it is possible to notice that, despite similar behaviour of the same configurations of different types of mirrors, the TY2 mirrors are worse than TY1, both in terms of temperature and deformation. The average of the maximum temperatures increases by 27 % (from 29.2 °C to 37.2 °C) corresponding to a relative increase of the average maximum absorbed power by 80 %. The average of the maximum total deformation rises by 33 % (from 0.085 mm to 0.113 mm). Such a difference is visible in Figs. 6–7. A maximum temperature of the 1st flat P mirror TY2 43 % higher leads to a maximum total deformation 26 % higher.

This can be explained by considering two conditions. The first one is the geometry: the TY2 mirrors are smaller than the TY1 ones, so there is less material conducting heat and a lower stiffness. The second condition is the higher heat flux, which depends on the higher absorption coefficient, that changes as a function of propagating beam parameters, like the wave polarization.

Figs. 8 and 9 show the contour plots of the temperature (8) and total deformation (9) on the mirrors. These plots serve to compare the TY1 and TY2 and the three configurations of the mirror (for TY2 parallel configuration only the first mirror is reported) at the instant of the end of the pulse.

The distributions align with the findings presented in Table 4, where TY2 mirrors exhibit a higher overall temperature and consequently more deformation compared to TY1. In the temperature plots, it is evident that

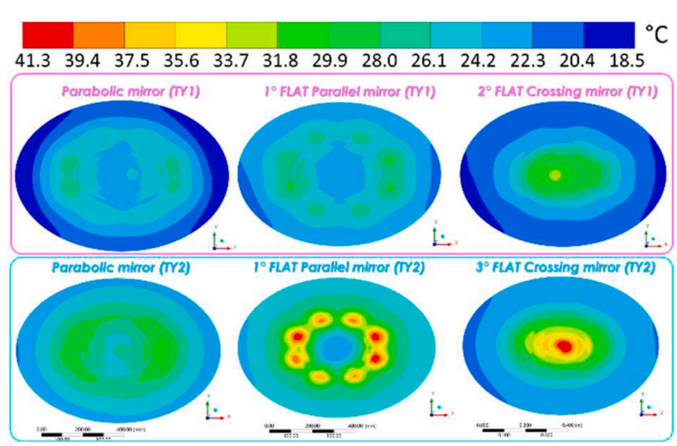

Fig. 8. Contour plots of the temperature distribution of the main mirror configurations.

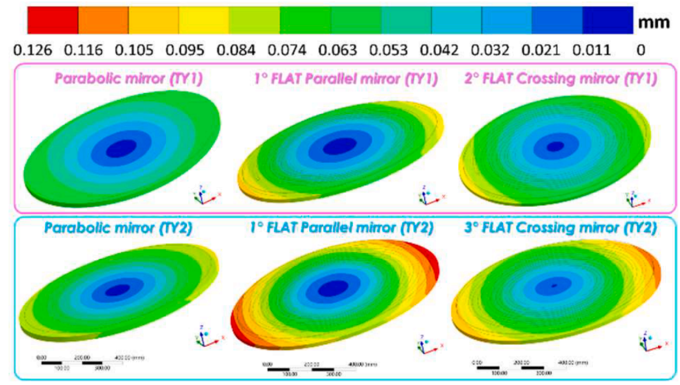

Fig. 9. Contour plots of the total deformation of the main mirror configurations (Scale factor: x400).

the crossing configurations, characterized by closer beams, display cooler edges with a temperature peak at the centre.

The maximum water temperature is higher in the external channel than the internal one, mainly due to the longer path. However, the flat C mirrors exhibit the opposite phenomenon, due to the distribution of the heat flux. On average, the water outlet temperatures for the external channel are approximately 26 °C (TY2) and 23 °C (TY1), while the internal channel's average water outlet temperatures are around 21.3 °C (TY2) and 22 °C (TY1).

In the end, it is useful to analyse a further comparison, presented in Fig. 10, where the Z-directional deformation on the major axis is reported for all the mirrors at the end of the pulse duration. This kind of deformation is the worst for the beam reflection due to changes in the focusing property of the mirror, which has been designed to grant the best propagation. Again, from Fig. 10, it is visible that the flat mirrors present higher deformations, and the TY2 (continue lines) are the worst. The maximum value of the 1st flat P mirror is about −0.083 mm. It is lower than the total deformation (0.100 mm), demonstrating that the x and y deformation are not null, but much lower than the z-deformation.

4.2. *Effect of the deformations on the TL performance*

The main outcomes of the analyses so far presented are the deformed profiles of the mirror reflective surfaces. They can be used in the electromagnetic software GRASP [16], which allows to calculate and compare the degradation of quality of the beam during the propagation in the case of undeformed mirrors and deformed ones. Preliminary results are reported in [6]. They concern the simulations performed for a modular unit of the MBTL (8 mirrors: 4 flat and 4 parabolic), in which the spurious mode fraction, in the propagating beams, increases by a factor of 3.5 when the deformed case is compared to undeformed one.

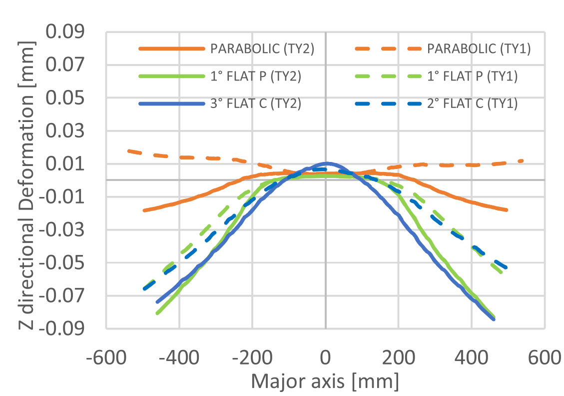

Fig. 10. Comparison of the trends of the Z-directional deformation on the major axis of the main mirror configurations.

The evaluation of the complete set of deformation expected along the TL is thus crucial to identify the mitigation actions to reduce the spurious mode content that would be unacceptably high when the effect of all the MBMs will be simulated. These actions, with the aim to reduce the mirror deformations, may encompass strategies such as leveraging higher pressure drops, optimizing cooling mechanisms, or, if necessary, reinforcing the mirrors' structural rigidity.

5. Conclusions

The conceptual design of the mirrors of the MBTL of DTT is presented. Building upon the conceptual design of the parabolic mirror presented in [11], in this work other mirror configurations are analysed, now completing the picture with a comprehensive examination of all MBMs configurations. Due to different thermal loads and dimensions, the temperature distribution and the maximum values are different between the mirrors TYPE 1 (midsection of the MBTL) and those TYPE 2 (beginning and end of the MBTL). Such differences affect the deformations: the TYPE 2 mirrors deform more than the others.

Specifically, a 43 % increase in the maximum temperature observed in the 1st flat P mirror of TYPE 2 corresponds to a 26 % higher maximum total deformation when compared to TYPE 1 mirror. Considering the structural simulations, the deformed reflective surfaces are obtained. They are used as input for the electromagnetic simulations to analyse the beam propagation and to calculate the contribution to the overall transmission losses, assessing whether the present deformations are acceptable or not. The first results show that mitigation actions are necessary to reduce the losses. Potential enhancements are ready to be considered, such as extending the path and reducing the spiral pitch (increasing the pressure drops within the limits) or reinforcing the mirrors' structural rigidity.

CRediT authorship contribution statement

A. Salvitti: Conceptualization, Data curation, Formal analysis, Methodology, Software, Visualization, Writing – original draft, Writing – review & editing. **A. Bruschi:** Conceptualization, Resources, Supervision, Validation, Writing – review & editing. **G. Calabrò:** Funding acquisition, Supervision, Validation. **F. Fanale:** Conceptualization, Investigation, Resources, Visualization, Writing – review & editing. **P. Fanelli:** Conceptualization, Funding acquisition, Methodology, Software, Supervision, Validation. **S. Garavaglia:** Resources, Writing – review & editing. **G. Granucci:** Project administration, Supervision. **S. Meloni:** Conceptualization, Formal analysis, Methodology, Visualization, Writing – original draft, Writing – review & editing. **A. Moro:** Conceptualization, Investigation, Resources, Supervision, Writing – review & editing. **P. Platania:** Formal analysis. **A. Romano:** Project administration, Supervision. **M. Scungio:** Supervision.

Declaration of competing interest

The authors declare that they have no known competing financial interests or personal relationships that could have appeared to influence the work reported in this paper.

Data availability

Data will be made available on request.

Acknowledgements

This work is carried out in the frame of the DTT activity. The authors are very grateful to all the colleagues involved in the DTT project for their precious contributions.

References

[1] R. Martone, et al., DTT Divertor Tokamak Test facility Interim Design Report, ENEA (2019).
[2] S. Garavaglia, et al., Progress of DTT ECRH system design, Fus. Eng. Des. 168 (2021) 112678.
[3] S. Garavaglia, et al., Development of the electron cyclotron resonance heating system for Divertor Tokamak Test, J. Vac. Sci. Technol. B 41 (2023) 044201.
[4] A. Bruschi, et al., Conceptual design of the DTT ECRH quasi-optical transmission line, Fus. Eng. Des. 194 (2023) 113727.
[5] F. Fanale, et al., 2023. Status of DTT ECH transmission lines and antennae, submitted to IEEE Transactions on Plasma Science.
[6] A. Moro, et al., 2024. Progress and challenges of the ECH transmission line design for DTT, submitted to Fusion Engineering and Design.
[7] S. Garavaglia, et al., Development of the multi-beam transmission line for DTT ECRH system, EPJ Web Conf. 277 (2023). EDP Sciences.
[8] L. Empacher, et al., Analysis of a multiple-beam waveguide for free-space transmission of microwaves, IEEE Trans. Antennas Propag. 49 (3) (2001) 483–493.
[9] V. Erckmann, et al., ECRH for W7-X: transmission losses of high-power 140 GHz wave beams, Fus. Sci. Technol. 55 (1) (2001) 16–22.
[10] P.F. Goldsmith, Quasioptical Systems, Wiley-IEEE Press Springer, US, 1998.
[11] A. Salvitti, et al., Preliminary thermal and structural analyses on the parabolic mirror of the Multi-Beam Transmission Line of the DTT ECH system, Fus. Eng. Des. 200 (2024) 114106.
[12] V. Erckmann, et al., Electron cyclotron heating for W7-X: physics and technology, Fusion Sci. Technol. 52 (2) (2007) 291–312.
[13] W. Kasparek, et al., Mirror development for the 140 GHz ECRH transmission system on the stellarator W7-X, Fus. Eng. Des. 53 (2001) 545–551, 1-4.
[14] H. Hailer, et al., Mirror development for the 140 GHz ECRH system of the stellarator W7-X, Fus. Eng. Des. 66 (2003) 639–644.
[15] A. Salvitti, et al., Preliminary design and thermal analyses of the steerable mirror cooling channel of the DTT ECRH, Fus. Eng. Des. 161 (2020) 111880.
[16] GRASP, Technical Description, TICRA. Knud Pontoppidan, 2017. (https://www.ticra.com/).